

Electronic structures, magnetic properties, and martensitic transformation in all-d-metal Heusler-like alloys Cd_2MnTM ($TM = \text{Fe, Ni, Cu}$)*

Yong Li(李勇)¹, Peng Xu(徐鹏)², Xiaoming Zhang(张小明)³,
Guodong Liu(刘国栋)³, Enke Liu(刘恩克)^{4,5}, and Lingwei Li(李领伟)^{1,2,†}

¹Institute of Advanced Magnetic Materials, School of Materials and Environmental Engineering, Hangzhou Dianzi University, Hangzhou 310012, China

²Key Laboratory of Electromagnetic Processing of Materials (Ministry of Education), Northeastern University, Shenyang 110819, China

³School of Materials Science and Engineering, Hebei University of Technology, Tianjin 300130, China

⁴Institute of Physics, Chinese Academy of Sciences, Beijing 100190, China

⁵Songshan Lake Materials Laboratory, Dongguan 523808, China

(Received 28 February 2020; revised manuscript received 7 May 2020; accepted manuscript online 28 May 2020)

The electronic structures, magnetic properties, and martensitic transformation in all-d-metal Heusler-like alloys Cd_2MnTM ($TM = \text{Fe, Ni, Cu}$) were investigated by the first-principles calculations based on density-functional theory. The results indicate that all three alloys are stabilized in the ferromagnetic $L2_1$ -type structure. The total magnetic moments mainly come from Mn and Fe atoms for Cd_2MnFe , whereas, only from Mn atoms for Cd_2MnNi and Cd_2MnCu . The magnetic moment at equilibrium lattice constant of Cd_2MnFe ($6.36 \mu_B$) is obviously larger than that of Cd_2MnNi ($3.95 \mu_B$) and Cd_2MnCu ($3.82 \mu_B$). The large negative energy differences (ΔE) between martensite and austenite in Cd_2MnFe and Cd_2MnNi under tetragonal distortion and different uniform strains indicate the possible occurrence of ferromagnetic martensitic transformation (FMMT). The minimum total energies in martensitic phase are located with the c/a ratios of 1.41 and 1.33 for Cd_2MnFe and Cd_2MnNi , respectively. The total moments in martensitic state still maintain large values compared with those in cubic state. The study is useful to find the new all-d-metal Heusler alloys with FMMT.

Keywords: all-d-metal Heusler-like alloys, electronic structures, magnetic properties, martensitic transformation

PACS: 71.15.Mb, 31.15.A-, 71.20.-b, 75.20.En

DOI: 10.1088/1674-1056/ab9739

1. Introduction

The ferromagnetic Heusler-based shape memory alloys (FSMAs)^[1] which is a large family of multifunctional materials have been well studied both theoretically and experimentally. Introducing the external fields, the martensitic transformation (MT) will happen with the change of magnetic states from ferromagnetic (FM) state and antiferromagnetic/paramagnetic (AFM/NM) state. In the process of FMMT, there are usually accompanied by various physical properties, such as magnetic-field-induced recovery, magnetocaloric effect, barocaloric effect, exchange bias, magnetoresistance, and magnetostrain.^[2–19]

Recently, the all-d-metal Heusler-like alloys based on d-d hybridization by substituting transition metal (TM) with less valence electrons for main group element in classic Heusler alloys were reported.^[20,21] The metamagnetic MTs and corresponding multifunctional properties (magnetic-entropy change,^[20] field-induced strain,^[21] giant elastocaloric effect^[11,22,23]) were gained in $\text{MnNiTi}(\text{Co})$ system. Wei^[22] reported a reversible elastocaloric effect with $\Delta T_{ad} = 9.0$ K at a

strain level of 4.6% for $\text{Ni}_{35}\text{Co}_{15}\text{Mn}_{35}\text{Ti}_{15}$. Aznar^[23] reported a giant barocaloric effect for $\text{Ni}_{50}\text{Mn}_{31.5}\text{Ti}_{18.5}$, which has maximum value of adiabatic temperature (12 K) and isothermal entropy changes ($74 \text{ J}\cdot\text{kg}^{-1}\cdot\text{K}^{-1}$) under 4 kbar (1 bar = 10^5 Pa). More ferromagnetic MT behaviors^[24–26] were also reported in other $\text{MnNiTi}(\text{Co})$ system. The exploration and design of new all-d-metal Heusler alloys has become a research hotspot.

Afterward, the crystal and electronic structures and MTs were predicted in Mn-based, Ni-based, and Pd-based all-d-metal Heusler alloys by first-principles calculations.^[27–30] Among the Heusler-based alloys, the Zn-based and Cd-based materials are less investigated in comparison with the other d-metals. This is probably due to the high vapor pressure (low boiling point)^[31–33] of these metals which makes them difficult to be fabricated. Thus the first-principles calculations become an effective method to predict crystal structure and phase stability. Recently, Han *et al.*^[34] found that the Zn_2MnTM crystalize $L2_1$ -type structure with ferromagnetic state, Zn_2RuMn , Zn_2RhMn , Zn_2OsMn , and Zn_2IrMn have possible MT. Yang *et al.*^[35] reported the atomic configura-

*Project supported by the Natural Science Foundation of Zhejiang Province, China (Grant No. LQ19E010006), the National Natural Science Foundation of China (Grant Nos. 51671048 and 91963123), the Ten Thousand Talents Plan of Zhejiang Province, China (Grant No. 2018R52003), and the Fundamental Research Funds for the Provincial University of Zhejiang Province, China (Grant No. GK199900X022).

†Corresponding author. E-mail: lingwei@hdu.edu.cn

tions, electronic, magnetic, mechanical, and dynamic properties for $\text{Cr}_2\text{ZnSi}/\text{Cr}_2\text{ZnGe}$.

In this work, we investigated the electronic structures, magnetic properties, and martensitic transformation in Cd-based all-d-metal Heusler-like alloys Cd_2MnTM ($TM = \text{Fe}, \text{Ni}, \text{Cu}$) by first-principles calculations. And we found that three samples reveal the ferromagnetic state with L_{21} -type structure, and the Cd_2MnFe and Cd_2MnNi may possess the ferromagnetic martensitic transformation.

2. Computational methods

The Cambridge Serial Total Energy Package (CASTEP) code, based on pseudopotential method with a plane-wave basis set, was used to investigate the electronic structures, magnetic properties, and MT of all-d-metal Heusler-like alloys Cd_2MnTM ($TM = \text{Fe}, \text{Ni}, \text{Cu}$).^[36,37] The generalized-gradient-approximation (GGA)^[38] and ultra-soft pseudopotential^[36] were selected to carry out the electron-exchange-related energy and interaction between atomic core and valence electrons, respectively. A 500-eV plane basis set energy cut-off and the Monkhorst–Pack special $16 \times 16 \times 16$ k -point mesh were used in the irreducible Brillouin zone. The selected energy convergence and self-consistent field tolerances were within 1×10^{-6} eV/atom and 1×10^{-7} eV/atom, respectively.

3. Results and discussion

The classic full-Heusler alloys X_2YZ (X and Y are TM atoms, Z is main group atom) have the highly ordered structures, there are four atom sites occupied the atoms, namely, A (0,0,0), B (0.25,0.25,0.25), C (0.5,0.5,0.5), and D (0.75,0.75,0.75). Normally, there are two possible atomic-site orderings on the basis of the site rule of Heusler alloys.^[39,40]

The first is L_{21} -type structure, in which two X atoms with higher valence electrons prefer to occupy sites A and C , Y atom with fewer valence electrons prefers to occupy site B , main group atom Z prefers to occupy site D . The other is XA -type structure, in which two X atoms with fewer valence electrons prefer to occupy sites A and B , Y atom with higher valence electrons prefers to occupy site C , main group Z atom prefers to occupy site D . In our work, the main group atom Z is replaced by TM atom. The two crystal structures of Cd_2MnTM ($TM = \text{Fe}, \text{Ni}, \text{Cu}$) are shown in Fig. 1.

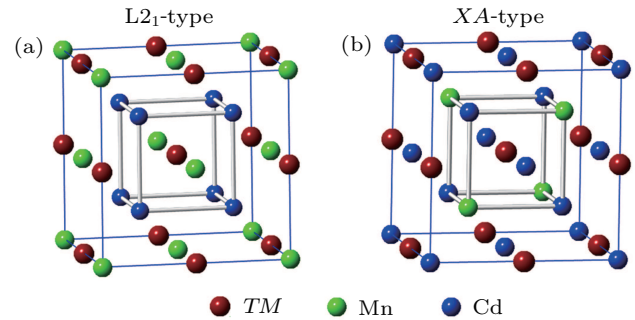


Fig. 1. (a) L_{21} -type and (b) XA -type crystal structures of Cd_2MnTM ($TM = \text{Fe}, \text{Ni}, \text{Cu}$) compounds.

The calculated total energy as a function of lattice constant for Cd_2MnTM ($TM = \text{Fe}, \text{Ni}, \text{Cu}$) is shown in Fig. 2. The ferromagnetic (FM), antiferromagnetic (AFM), nonmagnetic (NM) states in both crystal structures (L_{21} -type and XA -type) were considered to evaluate the ground state of Cd_2MnTM ($TM = \text{Fe}, \text{Ni}, \text{Cu}$) alloys through geometric optimization. The lowest energy for all the alloys appears with the L_{21} -type structure in FM state. The calculated equilibrium lattice constants are 6.49 Å, 6.44 Å, and 6.51 Å, respectively. The crystal structure, magnetic state, and equilibrium lattice constants are listed in Table 1. Therefore, we further select the FM L_{21} -type structure in subsequent discussions to study other properties.

Table 1. Crystal structure, equilibrium lattice constant (a), total and partial spin moments for Cd_2MnTM ($TM = \text{Fe}, \text{Ni}, \text{Cu}$) at equilibrium lattice constant.

Compound	Structure	$a/\text{Å}$	$M_{\text{tot}}/\mu_{\text{B}}$	$M_{\text{Cd}}/\mu_{\text{B}}$	$M_{\text{TM}}/\mu_{\text{B}}$	$M_{\text{Mn}}/\mu_{\text{B}}$
Cd_2MnFe	L_{21} -type	6.49	6.36	0.02	2.72	3.61
Cd_2MnNi	L_{21} -type	6.44	3.95	0.02	0.19	3.72
Cd_2MnCu	L_{21} -type	6.51	3.82	0.03	0.01	3.76

After geometric optimization, the band structures of L_{21} -type Cd_2MnTM ($TM = \text{Fe}, \text{Ni}, \text{Cu}$) alloys were calculated (see Fig. 3) at their equilibrium lattice constants in cubic state. Based on the band structures of three alloys, the bands in spin-up and spin-down channels overlap with the Fermi level (E_{F}) indicates that all the alloys are typical metallic characterization. The degrees of overlap in spin-up channel are approximately the same, but the degrees of overlap in spin-down channel are obviously different. This difference in electronic structures corresponds to a huge difference in magnetism. As we all

known, the electronic structures and magnetic properties are mainly determined by the electronics near E_{F} . Therefore, to further analyze magnetic properties, the calculated total density of states (TDOS) and partial density of states (PDOS) of L_{21} -type Cd_2MnTM ($TM = \text{Fe}, \text{Ni}, \text{Cu}$) were performed, which are shown in Fig. 4. For all TDOS, the spin-up and spin-down bands go across E_{F} . Between -10 eV and -7 eV, there are a couple of symmetrical peaks in the spin-up and spin-down states, which are far from the E_{F} and come from the Cd d-states. Therefore, the Cd d-states have weak contri-

butions to the total magnetic moments. For the region near Fermi level, the peaks appear at -4 eV to -1 eV in the spin-up direction and at -3 eV to $+2$ eV in the spin-down direction, which mainly come from the direct hybridizations between d-states of Mn and *TM*. The exchange splitting around the E_F of Cd_2MnFe in both spin states is stronger than that of Cd_2MnNi and Cd_2MnCu , since the spin-down DOS mainly locates above the Fermi level for Cd_2MnFe . Therefore, the spin magnetic moment of Cd_2MnFe is larger than that of other two alloys.

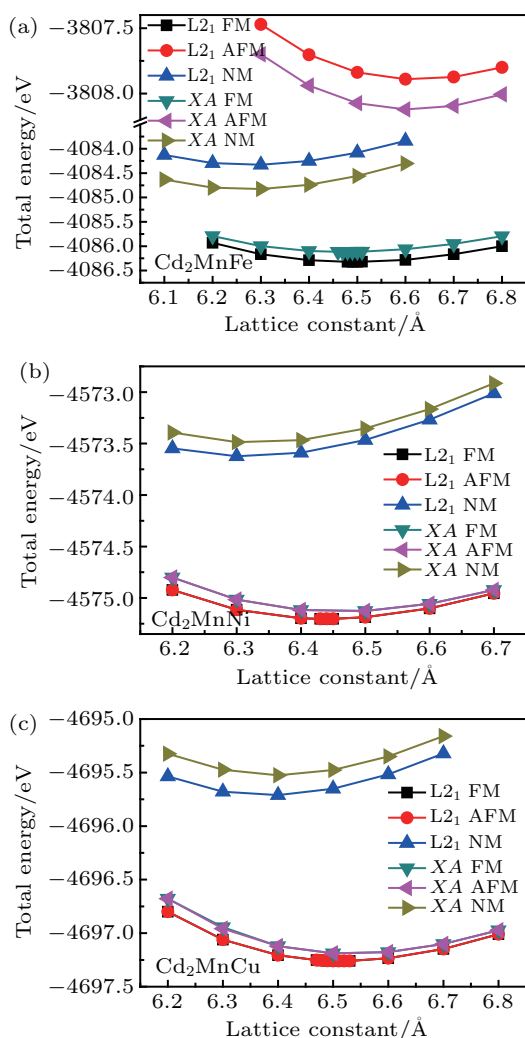


Fig. 2. Calculated total energy as a function of lattice constant for (a) Cd_2MnFe , (b) Cd_2MnNi , and (c) Cd_2MnCu with L21-type and XA-type structures in FM, AFM, and NM states, respectively.

Furthermore, the structure instability of Cd_2MnFe comes from the sharp peak near E_F due to the energy increasing of the system.^[41] The structures of Cd_2MnNi and Cd_2MnCu are relatively stable duo to the valleys appear near E_F based on Jahn–Teller effect,^[42] the aspect of MTs will be discussed in the subsequent section. For the PDOS, the d-states of Cd locate below -7 eV and the p-states with low energy locate in the energy region from -4 eV to $+2$ eV. There are strong d–d orbital hybridizations between Mn and *TM* atoms from -4 eV to $+2$ eV. The hybridization between the p states of Cd and d

states of other transition metal atoms can be expected. The Cd element acts as the main group element in the Heusler alloys, which is similar to Ga-based Heusler alloys.^[43] From the Fig. 4(a), the spin-down DOS mainly locates above the Fermi level, while the spin-up DOS mainly locates below the Fermi level, which results in the large spin splitting in two spin states for both Mn and Fe atoms and large spin magnetic moments from Mn and Fe atoms ($3.61 \mu_B$ and $2.72 \mu_B$, see Table 1), respectively. Therefore, Mn and Fe atoms make contributions considerably to the total magnetic moment. From Fig. 4(b) for Cd_2MnNi and Fig. 4(c) for Cd_2MnCu , compared with Mn atom, the Ni/Cu atom shows a relatively weak spin splitting in two spin states, there are a little spin magnetic moments from Ni and Cu atoms ($0.19 \mu_B$ and $0.01 \mu_B$, see Table 1), respectively. The total magnetic moments of Cd_2MnNi and Cd_2MnCu are contributed by Mn atoms only.

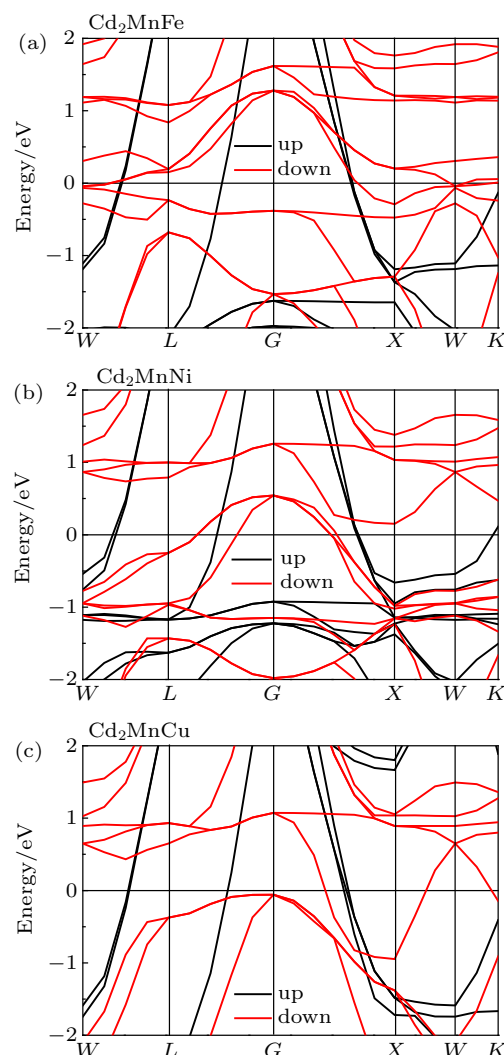


Fig. 3. Calculated band structures of L21-type (a) Cd_2MnFe , (b) Cd_2MnNi , and (c) Cd_2MnCu at each equilibrium lattice constant.

The total and atomic magnetic moments of L21-type (a) Cd_2MnFe , (b) Cd_2MnNi , and (c) Cd_2MnCu as a function of the lattice constant were calculated, as shown in Fig. 5. The total magnetic moments at equilibrium lattice constants are

$6.36 \mu_B$, $3.95 \mu_B$, $3.82 \mu_B$, respectively, which are listed in Table 1. With increasing the lattice constant, the total magnetic moments slightly increase and keep at large values. The values of magnetic moments are $3.5 \mu_B$ – $4.0 \mu_B$ for Mn atoms and $2.5 \mu_B$ – $3.0 \mu_B$ for Fe atoms (Fig. 5(a)).

moments of Ni atoms (Fig. 5(b)) and Cu atoms (Fig. 5(c)) are near zero. The results are consistent with the analysis of DOS. Large magnetic moments come from the spin splitting around the E_F for Mn and Fe atoms. All these make Cd_2MnFe having the largest total moment in the three alloys.

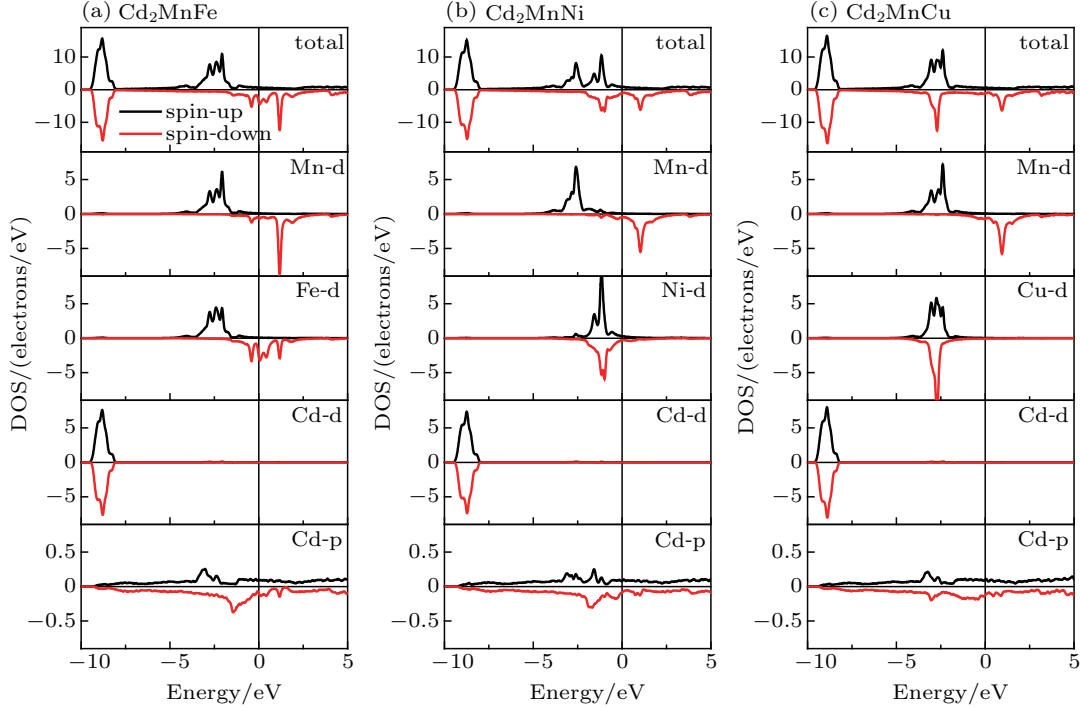


Fig. 4. Calculated total and partial density of states of L₂₁-type (a) Cd_2MnFe , (b) Cd_2MnNi , and (c) Cd_2MnCu at each equilibrium lattice constant.

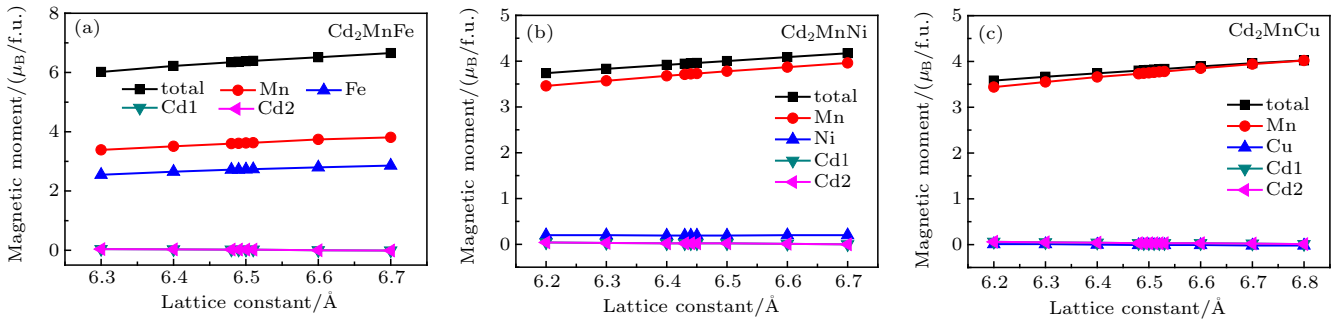


Fig. 5. Calculated total and atomic magnetic moments of L₂₁-type (a) Cd_2MnFe , (b) Cd_2MnNi , and (c) Cd_2MnCu as a function of the lattice constant.

To study the possibility of the MTs in Cd_2MnTM ($TM = \text{Fe, Ni, Cu}$) alloys, the energy difference (ΔE) between the tetragonal martensite and cubic austenite at the ground state as a function of c/a ratio (for c and a can be seen in Ref. [34]) with fixed crystal volumes, namely equilibrium cubic volume (V_{opt}) when $c/a = 1$, are given in Fig. 6. ΔE is a factor to determine whether the MT happens. The austenite is more stable than martensite when ΔE is less than zero, and vice versa. For Cd_2MnCu the minimum appears in $c/a = 1$, the ΔE is always above zero meaning that MT is unlikely to occur. The value of ΔE for Cd_2MnNi is the minimum (-0.04 eV) at $c/a = 1.33$. And for Cd_2MnFe , there are two minimum values, a shallow one in $c/a < 1$ and a deep one in $c/a > 1$. The shallow one is metastable phase, the most stable phase ap-

pears in $c/a = 1.41$ with the minimum (-0.19 eV). The negative values of ΔE imply that the alloys have a lower stability in austenitic phase, the total energy relax with changing the tetragonal distortion degree to a certain value of c/a , resulting in the MT happen for whole system.^[34,44,45] Therefore, Cd_2MnFe and Cd_2MnNi alloys would possess MTs. According to previous literature reports, the volume change based on the equilibrium lattice constant may influence the possible martensitic transformations,^[29,46] the energy difference (ΔE) as a function of c/a ratio with contraction/expansion of the unit cell volume ($V_{\text{opt}} + x\%V_{\text{opt}}$, $x = -3, -1, 0, 1, 3$), for Cd_2MnTM ($TM = \text{Fe, Ni}$) were studied. The corresponding data are given in Fig. 7. It can also be clearly seen that the possible MT occurs because the curves maintain with the change

of c/a for different x , the positions of metastable and most stable phases are unchanged. The value of ΔE decreases gradually from about -0.17 eV in the $+3\%$ volume phase to with about -0.21 eV in the -3% volume phase (inset of the Fig. 7), this can be a method for tuning the value of ΔE . It indicates that the -3% volume phase with $\Delta E = -0.21$ eV is the most stable one among the uniform strain range.

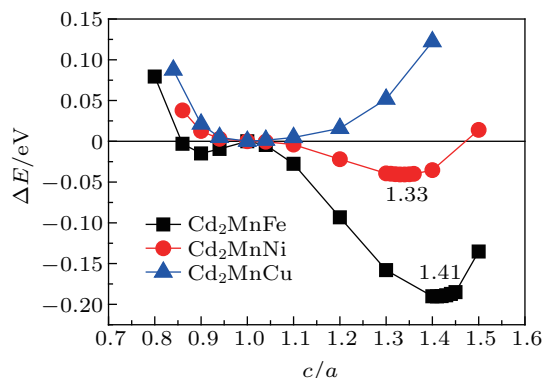


Fig. 6. ΔE as a function of the c/a ratio for Cd_2MnTM ($TM = \text{Fe}, \text{Ni}, \text{Cu}$). The zero point represents the energy of the austenite ($c/a = 1$).

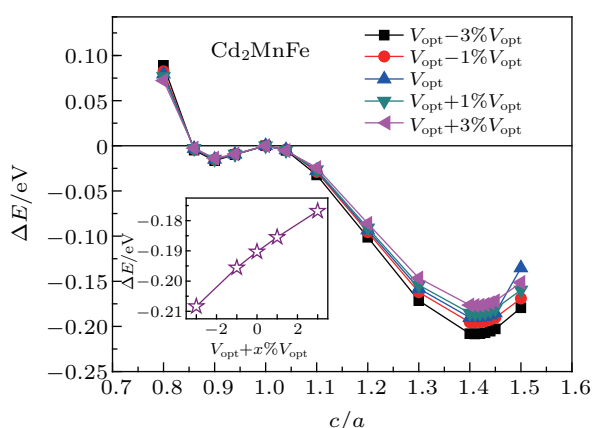


Fig. 7. ΔE as a function of c/a ratio for Cd_2MnFe with expansion/contraction of the unit cell volume. The zero point represents the energy of the austenite ($c/a = 1$). Inset: the relationship between ΔE and $V_{\text{opt}} + x\%V_{\text{opt}}$.

Considering the magnetic moments of Cd_2MnTM ($TM = \text{Fe}, \text{Ni}, \text{Cu}$) with fixed volume, we carried out the total and atomic moments in the change of c/a . The band structures of Cd_2MnFe with $c/a = 1.41$ and Cd_2MnNi with $c/a = 1.33$ are shown in Figs. 8(a) and 8(b), respectively. The results indicate that the two alloys still show ferromagnetic character due to the overlap between the Fermi level and the bands in spin-up and spin-down channels. The total magnetic moments in martensitic state decrease slightly compared to $c/a = 1$. Mn and Fe atoms make mainly contribution to total magnetic moments.

Figure 9 shows the total and atomic magnetic moments as function of c/a . With increasing the c/a , the total magnetic moment of Cd_2MnFe and atomic magnetic moments of Mn atom ($3.39 \mu_B - 3.81 \mu_B$) and Fe atoms ($2.55 \mu_B - 2.86 \mu_B$) are still large, which is preferable for the magnetostrictive behavior in martensitic state. The slightly decrease comes

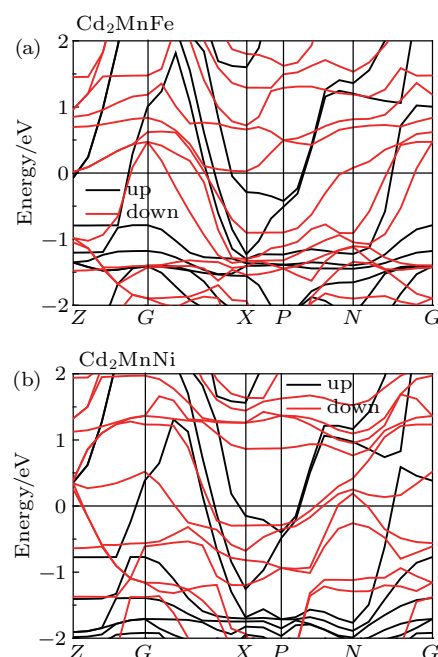


Fig. 8. (a) Calculated band structure of Cd_2MnFe with $c/a = 1.41$. (b) Calculated band structure of Cd_2MnNi with $c/a = 1.33$.

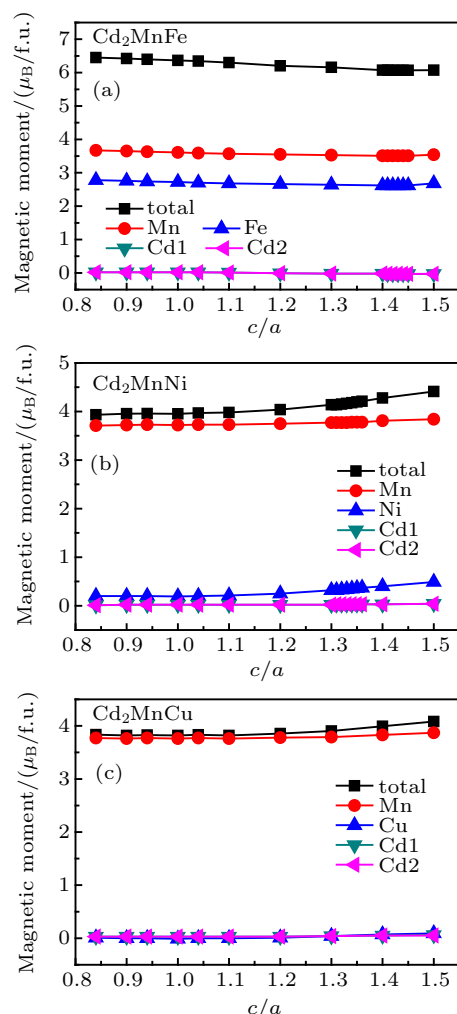


Fig. 9. Calculated total and atomic magnetic moments of L2₁-type (a) Cd_2MnFe , (b) Cd_2MnNi , and (c) Cd_2MnCu as a function of c/a .

from decline of the magnetic moments of Fe and Mn atoms in martensitic state. For Cd_2MnNi and Cd_2MnCu , the values

of total magnetic moments are stable in the c/a range of 0.85–1.10, increase of magnetic moments of Ni atoms for Cd_2MnNi and Mn atoms for Cd_2MnCu gives rise to slightly increase of total magnetic moments above $c/a > 1.2$. The magnetic moments of Cu and Cd atoms are almost unchanged (near zero) showing that it is insensitive to the change of c/a . Therefore, among the changing of c/a , total magnetic moments of Cd_2MnTM ($TM = \text{Fe}, \text{Ni}, \text{Cu}$) still maintain large values due to the robust ferromagnetic exchange interaction. The total and partial magnetic moments of Cd_2MnTM ($TM = \text{Fe}, \text{Ni}$) in their martensitic phases are listed in Table 2.

Table 2. Energy difference ΔE between martensite and austenite, c/a ratio, total and partial magnetic moments of Cd_2MnTM ($TM = \text{Fe}, \text{Ni}$) in their martensitic phases.

Compound	$\Delta E/\text{eV}$	c/a	$M_{\text{tot}}/\mu_{\text{B}}$	$M_{\text{Cd}}/\mu_{\text{B}}$	$M_{\text{TM}}/\mu_{\text{B}}$	$M_{\text{Mn}}/\mu_{\text{B}}$
Cd_2MnFe	-0.19	1.41	6.07	-0.03	2.62	3.51
Cd_2MnNi	-0.04	1.33	4.17	0.03	0.34	3.77

4. Conclusions

In summary, we have studied the electronic structures, magnetic properties, and martensitic transformation in all-d-metal Heusler-like alloys Cd_2MnTM ($TM = \text{Fe}, \text{Ni}, \text{Cu}$) by first-principle calculations. The ferromagnetic $L2_1$ -type cubic structure is the most stable phase. Applying site rule of Heusler alloys, the two Cd atoms prefer to occupy the equilibrium A , C sites, Mn and TM atoms prefer to occupy the equilibrium B and D sites, respectively. The total magnetic moment at equilibrium lattice constant of Cd_2MnFe ($6.36 \mu_{\text{B}}$) is larger than Cd_2MnNi ($3.95 \mu_{\text{B}}$) and Cd_2MnCu ($3.82 \mu_{\text{B}}$). The energy differences (ΔE) between martensite and austenite are negative in Cd_2MnFe and Cd_2MnNi under tetragonal distortion and different uniform strains, indicating the possible occurrence of the ferromagnetic martensitic transformation. The present theoretical investigation in Cd_2MnTM alloys would provide some valuable information for exploring new all-d-metal Heusler alloys.

References

- [1] Webster P J, Ziebeck K R A, Town S L and Peak M S 1984 *Philos. Mag. B* **49** 295
- [2] Wang W H, Wu G H, Chen J L, Gao S X, Zhan W S, Wen G H and Zhang X X 2001 *Appl. Phys. Lett.* **79** 1148
- [3] Kainuma R, Imano Y, Ito W, Sutou Y, Morito H, Okamoto S, Kitakami O, Oikawa K, Fujita A, Kanomata T and Ishida K 2006 *Nature* **439** 957
- [4] Ullakko K, Huang J K, Kokorin V V and O'Handley R C 1997 *Scr. Mater.* **36** 1133
- [5] Liu J, Gottschall T, Skokov K P, Moore J D and Gutfleisch O 2012 *Nat. Mater.* **11** 620
- [6] Hu F, Shen B, Sun J and Wu G 2001 *Phys. Rev. B* **64** 132412
- [7] Mañosa L, González-Alonso D, Planes A, Bonnot E, Barrio M, Tamarit J L, Aksoy S and Acet M 2010 *Nat. Mater.* **9** 478
- [8] Nayak A K, Nicklas M, Chadov S, Khuntia P, Shekhar C, Kalache A, Baenitz M, Skourski Y, Guduru V K, Puri A, Zeitler U, Coey J M and Felser C 2015 *Nat. Mater.* **14** 679
- [9] Yu S Y, Liu Z H, Liu G D, Chen J L, Cao Z X, Wu G H, Zhang B and Zhang X X 2006 *Appl. Phys. Lett.* **89** 162503
- [10] Singh S, Rawat R, Muthu S E, D'Souza S W, Suard E, Senyshyn A, Banik S, Rajput P, Bhardwaj S, Awasthi A M, Ranjan R, Arumugam S, Schlögl D L, Lograsso T A, Chakrabarti A and Barman S R 2012 *Phys. Rev. Lett.* **109** 246601
- [11] Cong D, Xiong W, Planes A, Ren Y, Mañosa L, Cao P, Nie Z, Sun X, Yang Z, Hong X and Wang Y 2019 *Phys. Rev. Lett.* **122** 255703
- [12] Wu M, Han Y, Bouhemadou A, Cheng Z, Khenata R, Kuang M, Wang X, Yang T, Yuan H and Wang X 2019 *IUCrJ* **6** 218
- [13] Zhao W Q, Dai X F, Zhang X M, Mo Z J, Wang X T, Chen G F, Cheng Z X and Liu G D 2019 *IUCrJ* **6** 552
- [14] Zhang Y J, Liu Z H, Wu Z G and Ma X Q 2019 *IUCrJ* **6** 610
- [15] Liu Z H, Tang Z J, Tan J G, Zhang Y J, Wu Z G, Wang X T, Liu G D and Ma X Q 2018 *IUCrJ* **5** 794
- [16] Li Y, Dai X, Liu G, Wei Z, Liu E, Han X, Du Z, Xi X, Wang W and Wu G 2018 *Chin. Phys. B* **27** 026101
- [17] Wang D, Wang C, Yu T and Liu W 2020 *Chin. Phys. B* **29** 043103
- [18] He C, Tang Y, Li X, He Y, Lu C and Guo Z 2019 *Chin. Phys. B* **28** 117501
- [19] Hao J, Hu F, Yu Z, Shen F, Zhou H, Gao Y, Qiao K, Li J, Zhang C, Liang W, Wang J, He J, Sun J and Shen B 2020 *Chin. Phys. B* **29** 047504
- [20] Wei Z Y, Liu E K, Chen J H, Li Y, Liu G D, Luo H Z, Xi X K, Zhang H G, Wang W H and Wu G H 2015 *Appl. Phys. Lett.* **107** 022406
- [21] Wei Z Y, Liu E K, Li Y, Han X L, Du Z W, Luo H Z, Liu G D, Xi X K, Zhang H W, Wang W H and Wu G H 2016 *Appl. Phys. Lett.* **109** 071904
- [22] Wei Z Y, Sun W, Shen Q, Shen Y, Zhang Y F, Liu E K and Liu J 2019 *Appl. Phys. Lett.* **114** 101903
- [23] Aznar A, Gràcia-Condal A, Planes A, Lloveras P, Barrio M, Tamarit J L, Xiong W, Cong D, Popescu C and Mañosa L 2019 *Phys. Rev. Mater.* **3** 044406
- [24] Yu K, Liu K, Ma S, Han X, Zhang Z, Song Y, Zhang Y, Chen C, Luo X and Zhong Z 2019 *J. Magn. Magn. Mater.* **484** 31
- [25] Liu K, Ma S, Ma C, Han X, Yu K, Yang S, Zhang Z, Song Y, Luo X, Chen C, Rehman S U and Zhong Z 2019 *J. Alloys Compd.* **790** 78
- [26] Liu K, Han X, Yu K, Ma C, Zhang Z, Song Y, Ma S, Zeng H, Chen C, Luo X, Rehman S U and Zhong Z 2019 *Intermetallics* **110** 106472
- [27] Wang X, Cheng Z, Liu G, Dai X, Khenata R, Wang L and Bouhemadou A 2017 *IUCrJ* **4** 758
- [28] Duan J, Wang Y, Zhang A, Liu S and Dar S A 2019 *Solid State Commun.* **290** 12
- [29] Han Y, Wu M, Feng Y, Cheng Z, Lin T, Yang T, Khenata R and Wang X 2019 *IUCrJ* **6** 465
- [30] Ni Z, Ma Y, Liu X, Luo H, Liu H and Meng F 2018 *J. Magn. Magn. Mater.* **451** 721
- [31] Li L W 2016 *Chin. Phys. B* **25** 037502
- [32] Zhang Y K 2019 *J. Alloys Compd.* **787** 1173
- [33] Li L and Yan M 2020 *J. Alloys Compd.* **823** 153810
- [34] Han Y, Bouhemadou A, Khenata R, Cheng Z, Yang T and Wang X 2019 *J. Magn. Magn. Mater.* **471** 49
- [35] Yang T, You J, Hao L, Khenata R, Wang Z and Wang X 2020 *J. Magn. Magn. Mater.* **498** 166188
- [36] Vanderbilt D 1990 *Phys. Rev. B* **41** 7892
- [37] Segall M D, Lindan P J D, Probert M J, Pickard C J, Hasnip P J, Clark S J and Payne M C 2002 *J. Phys.: Condens. Matter* **14** 2717
- [38] Perdew J P, Burke K and Ernzerhof M 1996 *Phys. Rev. Lett.* **77** 3865
- [39] Graf T, Casper F, Winterlik J, Balke B, Fecher G H and Felser C 2009 *Z. Anorg. Allg. Chem.* **635** 976
- [40] Skaftouros S, Özdoğan K, Şaşıoğlu E and Galanakis I 2013 *Phys. Rev. B* **87** 024420
- [41] Tan J G, Liu Z H, Zhang Y J, Li G T, Zhang H G, Liu G D and Ma X Q 2019 *Results Phys.* **12** 1182
- [42] Zeng Q, Shen J, Zhang H, Chen J, Ding B, Xi X, Liu E, Wang W and Wu G 2019 *J. Phys.: Condens. Matter* **31** 425401
- [43] Chen J, Liu E, Qi X, Luo H, Wang W, Zhang H, Wang S, Cai J and Wu G 2014 *Comp. Mater. Sci.* **89** 130
- [44] Faleev S V, Ferrante Y, Jeong J, Samant M G, Jones B and Parkin S S P 2017 *Phys. Rev. Appl.* **7** 034022
- [45] Entel P, Siewert M, Gruner M E, Chakrabarti A, Barman S R, Sokolovskiy V V and Buchelnikov V D 2013 *J. Alloys Compd.* **577** S107
- [46] Han Y, Wu M, Kuang M, Yang T, Chen X and Wang X 2018 *Results Phys.* **11** 1134